July 17, 1997

Formation of Light-quark Resonances in Two-Photon Collisions at LEP

The L3 Collaboration

Abstract

The two-photon partial widths of several light-quark resonances formed in $\gamma\gamma$ collisions have been measured in the L3 detector at LEP. For the decay channel $\pi^+\pi^-\gamma$, the Q^2 dependence and the form factor of the $\eta'(958)$ have been measured. The $\pi^+\pi^-\pi^0$ final state is dominated by the $a_2(1320)$ meson; there is also evidence for a radially excited state, $a_2'(1750)$ of $\mathrm{J}^{\mathrm{P}}=2^+$, produced predominantly in the helicity $\lambda = 2$ channel. The $f_2'(1525)$ is analyzed in the channels $K_s^0 K_s^0$ and K^+K^-.

Submitted to :
EPS 1997 summer conference, Jerusalem.
Abstract # 474

1 Introduction

The L3 detector [1] has the capability to measure charged particles and low momentum photons for the study of two-photon interactions $e^+e^- \to e^+e^-\gamma^*\gamma^*$, $\gamma^*\gamma^* \to X$. The process is particularly useful in the study of the properties of hadron resonances. The quantum numbers of the resonances are confined by the initial state of the two quasi-real photons. A neutral, unflavored meson with even charge conjugation and helicity zero or two can be formed. The resonance formation in two-photon collisions is described as the product of the two-photon luminosity function [2] for the transverse photon flux and the resonance cross section given by the Breit-Wigner formula. In the following we discuss the resonance formation for η' of $\mathrm{J^{PC}}=0^{-+}$ in $\pi^+\pi^-\gamma$ final state, the tensor mesons ($\mathrm{J^{PC}}=2^{++}$) a_2 in $\pi^+\pi^-\pi^0$ final state, and f_2, f_2' in $K^0_sK^0_s$, $\pi^+\pi^-$, K^+K^- final states.

2 The $\pi^+\pi^-\gamma$ final state

The formation of the $\eta'(958)$ is studied in the reaction $e^+e^- \to e^+e^-\eta'$, $\eta' \to \pi^+\pi^-\gamma$ [3]. The four-momentum transfers of the scattered electrons, q^2 and k^2, are often so small that the electrons go undetected along the beam. The photon with highest virtuality defines the variable $Q^2 = -q^2$. If one of the electrons is detected, the event is said to be *tagged*. The strength of the coupling of a meson to two photons, $\Gamma_{\gamma\gamma}$, and the Q^2 dependence of the formation cross section give information on the quark content and on the quark dynamics of the bound state. The Q^2 dependence of the cross section is expressed by the meson electromagnetic form factor F of

$$\sigma(W_{\gamma\gamma}, q^2, k^2) = \frac{1}{4}\sqrt{X} \cdot F^2(q^2, k^2) \cdot \frac{\Gamma_{\eta'} m_{\eta'}}{(W^2_{\gamma\gamma} - m^2_{\eta'})^2 + m^2_{\eta'}\Gamma^2_{\eta'}}, \tag{1}$$

$$F^2(q^2, k^2) = \frac{64\pi}{m^3_{\eta'}}\Gamma_{\gamma\gamma}(\eta') \cdot [\frac{1}{1 - q^2/\Lambda^2}]^2 \cdot [\frac{1}{1 - k^2/\Lambda^2}]^2 , \tag{2}$$

where $W_{\gamma\gamma}$ is the resonance invariant mass, $X = [(q \cdot k)^2 - q^2k^2]$ has the matrix elements for the coupling of pseudoscalar state to two virtual photon, Λ is related to the size of the meson [4] and must be described by any model of $q\bar{q}$ binding. Combining Eq. 1-2 leads a proportionality relation between the measured cross section and the two-photon width $\Gamma_{\gamma\gamma}(\eta')$.

The η' is a spin 0 particle. The decay $\eta' \to \rho\gamma$ corresponds to the transition $0^- \to 1^- + 1^-$ with the decay amplitude in the ρ rest frame of

$$\mathcal{M} = BW(\rho) \cdot \sqrt{2} m_{12} p^*_1 p^*_\gamma \sin\theta^*_1, \tag{3}$$

where m_{12} is the mass of the $\pi^+\pi^-$ system, p^*_γ is the photon momentum, p^*_1 is the π^+ momentum and θ^*_1 is the angle between the π^+ and the photon direction. Recently it has been claimed [5–7] that a pure ρ Breit-Wigner term is not sufficient to describe the data. A non-resonant contribution in the $\eta' \to \pi^+\pi^-\gamma$ decay, associated with a possible contribution of the box anomaly, has been included by adding a second term to the ρ Breit-Wigner:

$$BW(\rho) = \frac{1}{(m^2_{12} - m^2_\rho) - im_{12}\Gamma_\rho} + \frac{\xi}{m_{\eta'}} exp(i\phi) \tag{4}$$

where ξ is the relative amplitude with phase angle ϕ. For the ρ mass dependent width Γ_ρ, the formula of Ref. [8] is used in the this analysis :

$$\Gamma_\rho = \Gamma_0 \left(\frac{p_1^*}{p_0}\right)^3 \frac{m_\rho}{m_{12}} \tag{5}$$

where $p_0 = \sqrt{m_\rho^2 - 4m_\pi^2}/2$ and $\Gamma_0 = 151.2$ MeV is the nominal width of the ρ meson [9].

The PC Monte Carlo generator [10] is used to generate the events. The events $e^+e^- \to e^+e^-R$ ($R = \eta', a_2$) are generated according to the luminosity function of Budnev et al [2]. The Breit-Wigner shape, the form factor and the decay of the system R are then implemented as described by Eq. 1-5. The resonance parameters are taken from Ref. [9], except for the value of $\Gamma_{\gamma\gamma}(\eta')$ which is set to 1 keV.

2.1 Event selection

The candidate $e^+e^- \to e^+e^-\pi^+\pi^-\gamma$ events are selected by requiring a) *two oppositely charged tracks* each of transverse momentum p_T greater than 130 MeV, and b) *one photon only* in the BGO calorimeter with an energy greater than 140 MeV separated by an angle greater than 10° from tracks. The total transverse momentum squared of the two charged tracks $|\vec{p}_T(\pi^+\pi^-)|^2$ must be greater than 0.001 GeV^2, to eliminate the lepton channels $e^+e^- \to e^+e^-l^+l^-$. The angle of the π^+ in the ρ helicity frame must be such that $|\cos\theta_1^*| < 0.94$; this reduces non-resonant background. The events are classified in three groups:

I. the events produced by quasi-real photons ($Q^2 < 0.01$ GeV^2);

II. the intermediate range ($0.01 \leq Q^2 \leq 0.9$ GeV^2) where the electron goes undetected and the Q^2 is measured from the transverse momentum of the η';

III. the singly tagged events where one electron is detected in the small angle electromagnetic calorimeter ($1.5 \leq Q^2 \leq 10.0$ GeV^2).

2.2 Quasi-real photons and $\Gamma_{\gamma\gamma}(\eta')$

For the group-I sample, the analysis is limited to photons observed in the polar angle range $45° \leq \theta \leq 135°$ and with $|\vec{p}_T(\pi^+\pi^-\gamma)|^2 < 0.01$ GeV^2. The $\pi^+\pi^-\gamma$ mass spectrum is shown in Fig. 1. A total of 6767 events are selected, where 2786 are in the η' region ($0.85 \leq M(\pi^+\pi^-\gamma) \leq 1.05$ GeV). The η' mass, obtained by a Gaussian fit, is 958 ± 1 MeV with $\sigma = 24 \pm 1$ MeV. The enhancement around 1250 MeV is due to the tensor meson, $a_2(1320)$, whose dominant decay mode is: $a_2 \to \pi^\mp\rho^\pm \to \pi^\pm\pi^\mp\pi^0 \to \pi^\pm\pi^\mp\gamma\gamma$. If one of the two photons is undetected, these events can pass the selection cuts.

The two-photon radiative width $\Gamma_{\gamma\gamma}(\eta')$ is determined by fitting the mass spectrum of Fig. 1 with the Monte Carlo distribution for the η', for the a_2 and a third order polynomial for the background. The fit minimizes a χ^2 function with expected value in each bin i of :

$$E_i = \Gamma_{\gamma\gamma}(\eta') \cdot N_i(\eta') + N_i(a_2) + B_i \tag{6}$$

where N_i are the Monte Carlo expectations for the η' and for the a_2. The free parameters are $\Gamma_{\gamma\gamma}(\eta')$ (the two-photon width in keV units) and the coefficients of the polynomial background, B_i. The fitted two-photon width thus obtained is $\Gamma_{\gamma\gamma}(\eta') = 4.17 \pm 0.10$ (stat.) ± 0.27 (sys.) keV for $\chi^2/dof = 131/121$.

The fit results are superimposed on the data in Fig. 1. The systematic uncertainty for the $\Gamma_{\gamma\gamma}$ measurement is 6.5 %. The main uncertainties come from the branching ratio of the $\eta' \rightarrow \rho\gamma$ and from the selection cuts: 4.3 % from the branching ratio, 4 % from the cut in the photon energy, 1 % from the cut in $|\vec{p}_T(\pi^+\pi^-\gamma)|^2$, 2 % for the trigger and 1 % for background subtraction.

The good resolution of the detector and the high statistics allow an accurate study of the ρ meson line shape in the $\eta'\rightarrow\rho\gamma$ decay. In Fig. 2 the uncorrected $\pi^+\pi^-$ mass spectrum is shown. The ρ line shape given by Eq. 4 and 5 with $\xi = 0$ has been studied by generating 15 Monte Carlo samples with $756 \leq m_\rho \leq 774$ MeV and 12 samples with $130 \leq \Gamma_\rho \leq 160$ MeV. By comparing the data to the Monte Carlo samples, the minimum of the χ^2 ($\chi^2 = 34$ for 32 dof, C.L.=37 %) is found for the values $m_\rho = 766 \pm 2$ MeVand $\Gamma_\rho = 150 \pm 5$ MeV.

With the same method the possibility of a non-resonant $\pi^+\pi^-$ contribution (Eq. 4) has been tested by varying the ξ and ϕ parameters. The best agreement with the data is for $\xi = 0$ and $\phi = 0$. The values obtained by previous analysis $\xi = 2.78$ and $\phi = -1.07$ [5] and $\xi \simeq 0.4$ and $\phi = 3.14$ [6,7] are disfavored with a χ^2 of 68 (C.L.$\sim 10^{-4}$) and 49 (C.L.=3 %) respectively, for 32 degrees of freedom.

2.3 η' transition form factor

The Monte Carlo simulation demonstrates that $Q^2 = |\vec{p}_T(\pi^+\pi^-\gamma)|^2$ within the experimental resolution. For the events of group-II, the data are subdivided into three Q^2 intervals (Fig. 3a-c). The narrow η' signal is clearly seen above the background. The number of η' events obtained by a fit of a gaussian, superimposed to a third order polynomial background, is given in Table 1.

The tagged events, group-III, are selected by requiring a shower in the small angle electromagnetic calorimeter with energy greater than 35 GeV. The cut $|\vec{p}_T(\mathrm{e}^{\pm}_{tag}\pi^+\pi^-\gamma)|^2 < 0.05$ GeV^2 is applied, where the $\mathrm{e}^{\pm}_{tag}$ is detected electron. The $\pi^+\pi^-\gamma$ mass spectrum of this class of events is shown in Fig. 3d. The η' signal has a good resolution ($\sigma = 26$ MeV) over a small background. These tagged events are subdivided into two Q^2 intervals in Table 1.

The cross section is measured in each Q^2 interval as listed in Table. 1. The total integrated luminosity is 129 pb^{-1} for untagged events and 100 pb^{-1} for tagged events. The average Q^2 is calculated by taking into account the Q^2 dependence of the spectrum with the Monte Carlo. The systematic uncertainty from the selection is the same in all groups. The uncertainty from the background subtraction varies from 6 % to 10 % for different Q^2 intervals.

The decrease of the cross section for larger Q^2 is due to the two-photon luminosity function, to the matrix element squared $\sqrt{X}$ and to the resonance form factor. Such effects are estimated by Monte Carlo with events generated by a flat form factor ($F(Q^2)/F(0) = 1$). The η' transition form factor is then calculated. The transition form factor is also corrected for the four momentum squared k^2 of the second photon. The effect is studied by generating events with different input Λ values ($0.77 - 1.01$ GeV) in Eq. 2. The corrected results are given in Table 1 and in Fig. 4. The effect of collinear initial state radiation on the form factor is found to be negligible; it is less than 1 % for group-II untagged events and 3 % for group-III tagged events. The five high Q^2 points are fitted with the form factor parameterization given in Eq. 2. In addition, the value at $Q^2 = 0$ is fixed to the measured value of $\Gamma_{\gamma\gamma}$. The Λ value obtained is

$$\Lambda = 0.900 \pm 0.046\ (\text{stat.}) \pm 0.022\ (\text{sys.})\ \text{GeV} \qquad \chi^2/dof = 0.7/4$$

It is illustrated in Fig. 4a. The systematic error is due to the error evaluated in each cross section point (1.6 %) and to the uncertainty of the two-photon width (1.9 %). If the virtuality of the second photon was neglected, the value of Λ would be 11 % lower. The effect of collinear initial state radiation on Λ is smaller than 1 %.

For pseudoscalar mesons π^0, η and η', there exist several models which describe the transition form factor. The Vector Dominance (VDM) hypothesis relates Λ to the mass of vector mesons ρ, ω, ϕ. Its prediction, $\Lambda = 0.83$ GeV [4], for a weighted average of the vector mesons contributions, is shown in Fig. 4b as a dashed line. It is consistent with our data. The QCD models predict the η' form factor considering the mixing of the singlet and octet components of the flavour SU(3) pseudoscalar nonet. Brodsky and Lepage interpolate between the $Q^2 = 0$ and $Q^2 \to \infty$ limits with the pole form of Eq. 2 giving a parameter $\Lambda_{\eta'} = 0.66$ GeV [4,11]. This prediction is drawn in Fig. 4b as a dotted line. In the hard scattering approach, R. Jacob et al. [12] consider also the transverse degree of freedom for the $q\bar{q}$ wave function and include the gluonic corrections in a Sudakov factor. Their calculation reproduces our high Q^2 data better. In order to cover the low and moderately high Q^2 region of the photon-meson transition form factor, V.V. Anisovich et al. [13] introduce the $q\bar{q}$ distribution function G_γ at the $\gamma q\bar{q}$ vertex similar to the pion distribution function G_π describing the $\pi q\bar{q}$ vertex; i.e. the photon is treated much like a vector meson. The η and η' transition form factors [14] were calculated. They also explore the possibility that the η and the η' contain an extra glueball component. Their predictions are given in Fig. 4a for a variable admixture of gluonium content. The measurement of the two-photon width agrees with 5 % - 10 % gluonium content but the measurement of the transition from factor favors no gluonium content.

Q^2 interval	$\langle Q^2 \rangle$	η' events	ε	$\Delta\sigma$	$(m^3_{\eta'}/64\pi)F^2(Q^2)$
(GeV^2)	(GeV^2)		(%)	(pb)	(keV)
0.0 – 0.01		2123 $\pm$ 53	2.8	1924 $\pm$ 48 $\pm$ 96	4.17 $\pm$ 0.10 $\pm$ 0.27
0.01 – 0.15	0.06	726 $\pm$ 47	3.7	510 $\pm$ 33 $\pm$ 37	3.51 $\pm$ 0.23 $\pm$ 0.25
0.15 – 0.30	0.23	123 $\pm$ 18	2.9	109 $\pm$ 16 $\pm$ 8	2.78 $\pm$ 0.41 $\pm$ 0.21
0.30 – 0.90	0.53	58 $\pm$ 11	1.7	88 $\pm$ 17 $\pm$ 8	1.50 $\pm$ 0.29 $\pm$ 0.13
1.50 – 2.50	1.90	17 $\pm$ 5	5.3	10.4 $\pm$ 3.3 $\pm$ 1.1	0.38 $\pm$ 0.12 $\pm$ 0.04
2.50 – 10.0	4.14	19 $\pm$ 6	10.3	6.1 $\pm$ 1.8 $\pm$ 0.6	0.11 $\pm$ 0.03 $\pm$ 0.01

Table 1: Number of η' events and cross sections $\Delta\sigma$ as a function of Q^2. The total acceptance and efficiency ε are given. In the last column the electromagnetic transition form factor, corrected for the virtuality of the second photon, is calculated for each $\langle Q^2 \rangle$. The first error is statistical and the second is systematic.

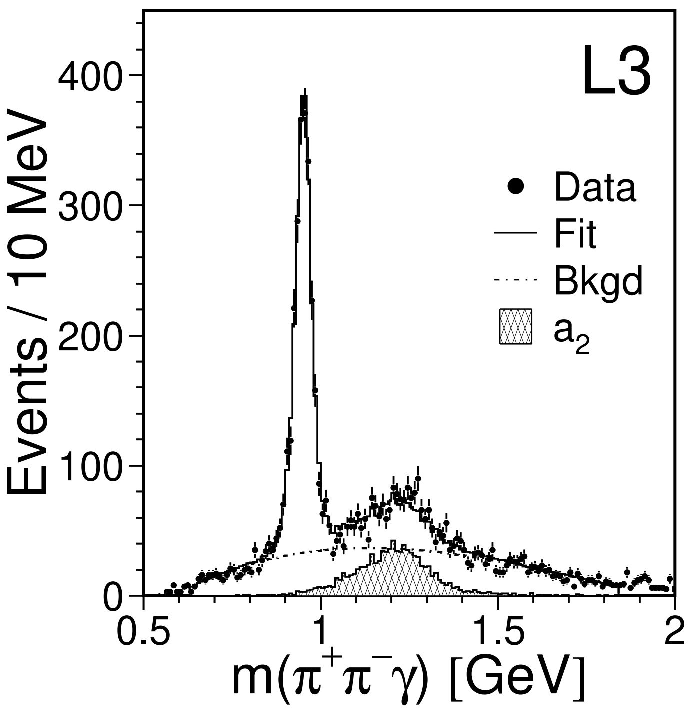

Figure 1: $\pi^+\pi^-\gamma$ mass spectrum for the events selected with $Q^2 < 0.01$ GeV^2 . The histogram is the result of the fit described in the text. The shaded area is the a_2 contribution, the dashed-dotted line the fitted third order polynomial background.

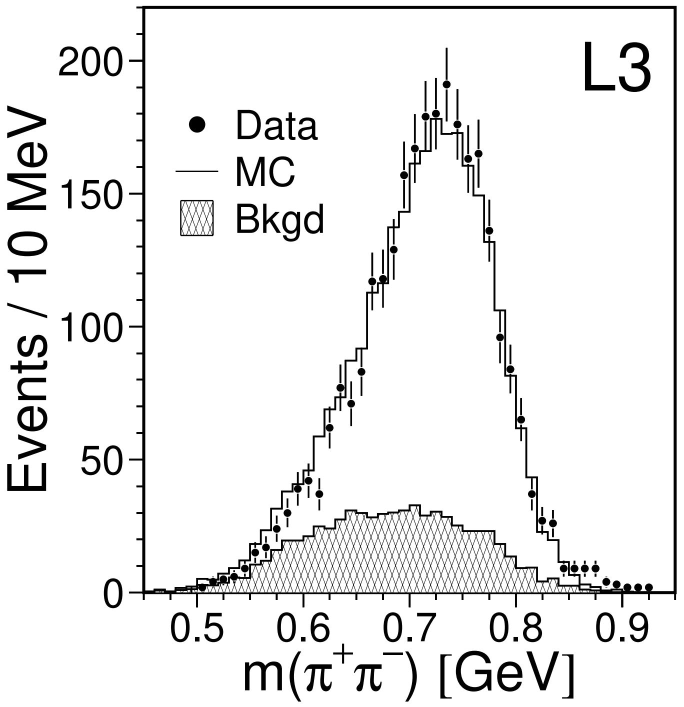

Figure 2: The uncorrected $\pi^+\pi^-$ effective mass distribution. The histogram is the prediction of the Monte Carlo which best fits the data ($m_\rho = 766$ MeV, $\Gamma_\rho = 150$ MeV and $\xi = 0$). The shaded area is the estimated background from a_2 and other inclusive processes simulated by assuming three-body phase space distribution.

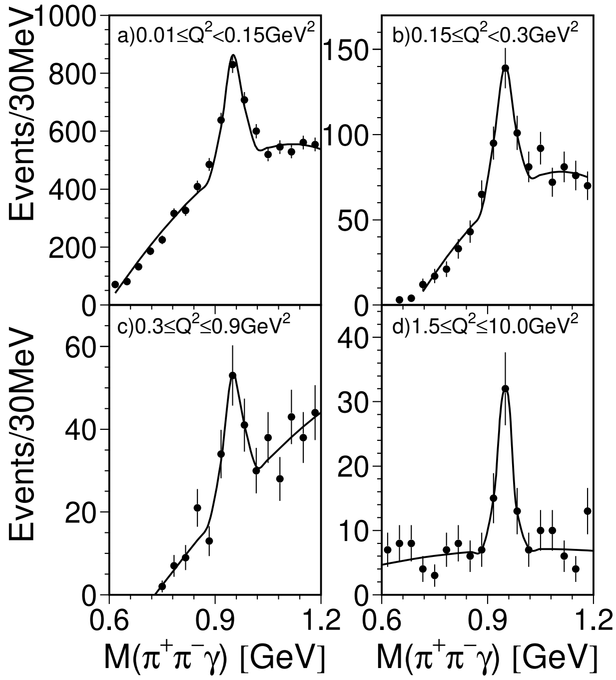

Figure 3: $\pi^+\pi^-\gamma$ mass for the events with high Q^2, separated in four Q^2 intervals: a) $0.01 \leq Q^2 < 0.15$ GeV^2, b) $0.15 \leq Q^2 < 0.30$ GeV^2, c) $0.30 \leq Q^2 \leq 0.90$ GeV^2, d) Tagged events, $1.5 \leq Q^2 \leq 10.0$ GeV^2.

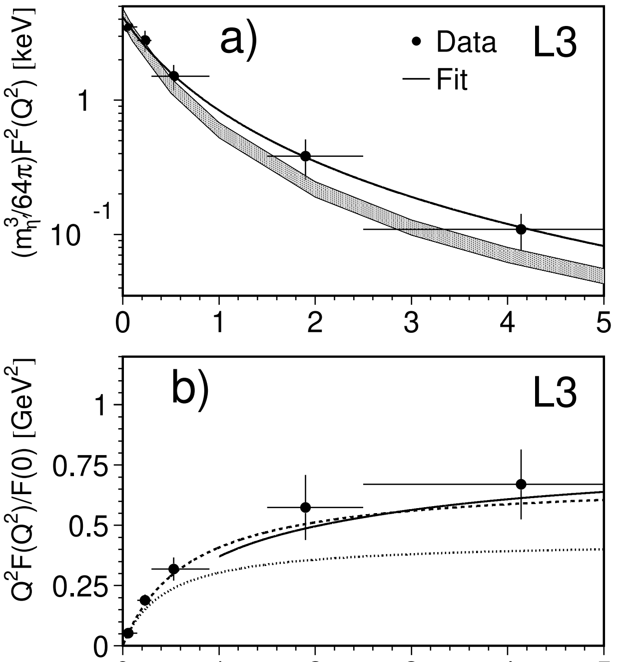

Figure 4: a) $F^2(Q^2)$ as measured at $\sqrt{s}$= 91 GeV. Statistical and systematic errors are added in quadrature. The solid line is the result of the pole fit to the data points described in the text. The predictions of Ref. [14] are indicated as a shaded area, ranging from no gluonium content (upper line) to 15 % of gluonium content (lower line). b) The same data are given as $Q^2F(Q^2)$, normalized to $F(Q^2 = 0)$. The data are compared to QCD calculations [12] (continuous line), to VMD predictions [4] (dashed line) and to Ref. [11] (dotted) line.

3 The $\pi^+\pi^-\pi^0$ final state

The $\pi^+\pi^-\pi^0$ final state in two-photon collisions is dominated by the $a_2(1320)$ meson with well established quantum numbers $J^{PC}=2^{++}$ decaying mostly into $\rho\pi$ [15]. The $\pi^+\pi^-\pi^0$ final state can be expressed as a set of two body intermediate states with orbital angular momentum L between a di-pion state and the third pion. The a_2 meson decays into $\pi^+\pi^-\pi^0$ through the $\rho^\pm\pi^\mp$ intermediate states with constructive interference [16]; $\rho^0\pi^0$ is forbidden by isospin invariance. For the decay of a candidate high-mass resonance, the intermediate states $\rho^\pm\pi^\mp$ and $f_2\pi^0$ are considered. The angular distribution depends on the spin-parity and helicity of the resonant state X. It is given by

$$\mathcal{T} = \sum_\lambda R_{\lambda\lambda} \left| \left(\frac{T_\lambda(X \to \rho^+\pi^- \to 3\pi)}{m_\rho^2 - s_+ - im_\rho\Gamma_\rho} + \frac{T_\lambda(X \to \rho^-\pi^+ \to 3\pi)}{m_\rho^2 - s_- - im_\rho\Gamma_\rho} \right) \right.$$
$$\left. + \alpha \exp(i\phi) \left(\frac{T_\lambda(X \to f_2\pi^0 \to 3\pi)}{m_{f_2}^2 - s_0 - im_{f_2}\Gamma_{f_2}} \right) \right|^2, \quad (7)$$

where $R_{\lambda\lambda}$ is the probability of the helicity λ state, $s_\pm, s_0$ are the invariant mass squared of the $\pi^\pm\pi^0, \pi^+\pi^-$ systems corresponding to $\rho^\pm$ and f_2. α is defined as the $\sqrt{BR(f_2\pi)/BR(\rho\pi)}$, and ϕ is the relative phase of the $f_2\pi$ and $\rho\pi$ decay amplitudes. For the a_2, α=0. The transition amplitude T_λ is given by

$$T_\lambda = 32\pi^2 \left(m_X\Gamma_X\, m_{2\pi}\Gamma_{2\pi} \frac{W_{\gamma\gamma}\sqrt{s_{2\pi}}}{p_{2\pi}p_\pi} \right)^{1/2} \times \sum_m C^{J\lambda}_{L,\lambda-m,l,m} Y_L^{\lambda-m}(\theta_{2\pi}, \phi_{2\pi}) Y_l^m(\theta_\pi, \phi_\pi), \quad (8)$$

where Γ_X is the X decay width at the resonance invariant mass $W_{\gamma\gamma}$, m_X is the resonance pole mass. The di-pion system has spin l with third component m, the invariant mass is $m_{2\pi}$ with the mass dependent width $\Gamma_{2\pi}$. The momentum, polar and azimuthal angles $(p_{2\pi}, \theta_{2\pi}, \phi_{2\pi})$ are measured in the $\gamma\gamma$ rest frame. The π from the di-pion decay has the corresponding variables $(p_\pi, \theta_\pi, \phi_\pi)$ measured in the di-pion rest frame. The angles in both frames are determined with respect to the $\gamma\gamma$ direction which is approximately the beam direction.

The Monte Carlo simulations use the PC [10] and TWOGEN [17] generators with a ρ dominated VMD form factor applied for the colliding photons. The mass and total width for the a_2 are taken from the Particle Data Group (PDG) [9]. In the high-mass range a Breit-Wigner resonance of mass 1740 MeV and total width 150 MeV have been assumed. Monte Carlo events were passed through a full detector simulation.

3.1 Event selection and background estimations

The process $e^+e^- \to e^+e^-\pi^+\pi^-\pi^0$ has been selected in an untagged configuration using data taken from 1991 to 1995 at a center-of-mass energy $\simeq$ 91 GeV. The corresponding integrated luminosity is 140.6 pb^{-1}. The p_T threshold for charged track selection is 60 MeV. The energy of a photon candidate is required to be greater than 80 MeV with an angular separation from charged tracks of $(\Delta\theta^2 + \Delta\phi^2)^{1/2} > 5.5°$. Photon candidates are selected in the angular regions $14° < \theta < 35°$, $45° < \theta < 135°$, or $145° < \theta < 166°$. The π^0 signal region is defined as $105 < m(\gamma\gamma) < 165$ MeV, where $m(\gamma\gamma)$ is the invariant mass of the two photons. The transverse momentum of the $\pi^+\pi^-\pi^0$ system relative to the beam direction is denoted by $\sum \vec{p}_T$. In the spin-parity-helicity analyses presented below, events with $|\sum \vec{p}_T|^2 < 0.0015$ GeV^2

are divided into two samples. The a_2 *low-mass* sample is selected with $\pi^+\pi^-\pi^0$ invariant mass of $1.0 < m(\pi^+\pi^-\pi^0) < 1.55$ GeV. The $\pi^\pm\pi^0$ invariant mass is required to be compatible with the ρ mass ($m(\pi^\pm\pi^0) < m_\rho + 250$ MeV) since the a_2 decays predominantly through the $\rho\pi$ intermediate state. The *high-mass* sample of $1.55 < m(\pi^+\pi^-\pi^0) < 2.1$ GeV is studied under the hypothesis of a resonance (or resonances) decaying through $\rho\pi$ and $f_2\pi$.

Fig. 5a to 5d show the $|\sum \vec{p}_T|^2$ distributions for different $\pi^+\pi^-\pi^0$ mass intervals. In the mass intervals 1.0-1.55 GeV and 1.55-2.1 GeV there is a clear excess of events at low $|\sum \vec{p}_T|^2$ corresponding to exclusive $\pi^+\pi^-\pi^0$ production. The almost flat background extending to large $|\sum \vec{p}_T|^2$ values is interpreted as inclusive production. The shaded histogram in Fig. 5c shows the prediction of a Monte Carlo phase space generation of the channel $\pi^+\pi^-\pi^0(\pi^0)$ where the last π^0 is unobserved. To estimate the statistical significance of the exclusive signals several fits were performed to the $|\sum \vec{p}_T|^2$ distributions below 0.02 GeV^2. The results and confidence levels of "background only" fits to a second order polynomial are given in the first two rows of Table 2. To estimate the levels of the inclusive backgrounds under the exclusive production signals in Figs. 5b,c the distributions were fitted to the sum of a Monte Carlo distribution including the effect of a ρ dominated Vector-Meson-Dominance (VMD) form factor to describe the exclusive signal, and a second order polynomial to describe the inclusive background. As listed in the third row of Table 2, acceptable fits are then obtained. The background levels for $|\sum \vec{p}_T|^2 < 0.0015$ GeV^2 of the fits are listed in the last three rows of Table 2.

mass region [GeV]	$0.60 - 1.00$	$1.00 - 1.55$	$1.55 - 2.10$	$2.10 - 2.50$
χ^2 (Background)	105	585	221	92
C.L.[%]	95	$< 10^{-6}$	1.1×10^{-4}	99
χ^2 (MC+Background)	–	157	155	–
C.L.[%]	–	5.4	6.7	–
Total events	42	618	184	38
Background events	–	120	46	–
Background fraction [%]	–	19 ± 0.5	25 ± 3	–

Table 2: The $|\sum \vec{p}_T|^2$ distributions below 0.02 GeV^2 in the four mass ranges are fitted to background only (first two rows) and Monte Carlo plus background (third and fourth rows). The χ^2 for 130 D.F. are listed. The fraction of background events in $|\sum \vec{p}_T|^2 < 0.0015$ GeV^2 are also listed with the number of events observed.

3.2 Spin-parity and helicity analysis

The *low-mass* sample is analyzed for the helicity state of the a_2. When produced in quasi-real two-photon collisions, the a_2 meson can have helicity states 0 or 2. The relative importance is determined by the least square minimization to the polar angle ($\cos\theta$) distributions of the final state pions in the resonance rest frame. The Monte Carlo expectations for the $\cos\theta$ distributions of π^0 and $\pi^\pm$ (two entries per event) are given by

$$E_i = P_b \cdot \mathcal{B}_i^\theta + P_{\gamma\gamma} \cdot \{P_2 \cdot M_i(2) + (1 - P_2) \cdot M_i(0)\} \tag{9}$$

where $M_i(\lambda)$ is the bin content of simulated events of helicity λ normalized to the expected number of events for a radiative width $\Gamma_{\gamma\gamma} = 1$ keV. The background distribution $\mathcal{B}_i^\theta$ is taken from the $\pi^+\pi^-\pi^0$ phase space Monte Carlo. The free parameters in the fit are the fraction P_2 of helicity 2 contribution, and the two scaling factors $P_{\gamma\gamma}$ for the radiative width of the resonance and P_b for the background contributions. The result of the fit is shown in Fig. 6. We have obtained $P_{\gamma\gamma} = 0.96 \pm 0.04$ and $P_2 = 0.92 \pm 0.05$ with $\chi^2/D.F. = 90/53$ (C.L.=0.11%). The total systematic uncertainty in P_2 is estimated to be 6% and has dominant contributions from background uncertainty and detector acceptance, each estimated to be 4%.

The *high-mass* sample is considered for the intermediate decay modes $\rho\pi$ and $f_2\pi$ with the coherent interference expressed in Eq. 7. We first analyze the spin-parity state using the Dalitz Λ parameter [18] defined in the $\pi^+\pi^-\pi^0$ rest frame by

$$\Lambda = \left| \frac{\mathbf{p}_{\pi^+} \times \mathbf{p}_{\pi^-}}{Q_K^2} \right|^2 \tag{10}$$

where the $\pi^\pm$ momenta ($\mathbf{p}_{\pi^\pm}$) are normalized to Q_K, the maximum possible kinetic energy for a pion in the event. The Λ distribution is shown as the data points in Fig. 7. It is sensitive to the distribution of the relative angles between the final state pions, and depends on the spin-parity of the state as well as the amplitude and phase parameters α and ϕ. A background level of 25% of inclusive events was used. Increasing either of these parameters in the Monte Carlo shifts the Λ distribution to lower values. The parameters α and ϕ are determined for each spin-parity and helicity state by minimizing the χ^2 value to the Monte Carlo expectations. The results of the fits are listed in Table 3. No acceptable fit was found for $2^-(0)$. The spin-parity $\mathrm{J^P} = 2^+$ is strongly favored. This fit is not, however, sensitive to the helicity state.

$\mathrm{J^P}(\lambda)$	$2^-(0)$	$2^+(0)$	$2^+(2)$
phase angle ϕ [deg.]	100	130 ± 18	170 ± 17
amplitude α	1.0	0.99 ± 0.10	0.97 ± 0.17
$\chi^2/15$ D.F.	3.94	0.83	0.61
C.L. [%]	3.6×10^{-5}	64	87

Table 3: Results of fits to the Λ distribution.

The helicity state can be 0 or 2 as for the a_2 with different angular distributions in the $\pi^+\pi^-\pi^0$ rest frame. Fig. 8 shows the $\cos\theta$ distributions for π^0 and $\pi^\pm$ (two entries per event). The data is fitted to Monte Carlo expectations of pure $2^-(0)$, $2^+(0)$, $2^+(2)$ states and inclusive $\pi^+\pi^-\pi^0(\pi^0)$ background :

$$E_i = P_b \cdot \mathcal{B}_i^\theta + P_{\gamma\gamma} \cdot \left\{(1 - F_{2^-})\left[P_2 M_i^+(2) + (1 - P_2)M_i^+(0)\right] + F_{2^-} M_i^-(0)\right\}. \tag{11}$$

The inclusive background is parameterized by $\mathcal{B}_i^\theta$ and scaled by P_b. $P_{\gamma\gamma}$ and P_2 are defined as in Eq. 9. The parameter F_{2^-} is the relative contribution of the $2^-(0)$ state. The results of the fits are listed in Table 4. Assuming a pure $2^-(0)$ state gives a low C.L. of 1.7×10^{-8} (column I). The fitted values of the background level and P_2 are $23 \pm 4\%$ and $77 \pm 12\%$ respectively (column II). The fitted background is consistent with that derived from the $|\sum \vec{p}_T|^2$ distributions ($25\pm3\%$, Table. 2). A fit is also performed with background level fixed at 23% and the $2^-(0)$ contribution left free (column III). The upper limit for a possible $2^-(0)$ contribution is $\Gamma_{\gamma\gamma}\mathrm{BR}(\pi^+\pi^-\pi^0) \leq 0.072$ keV (90% C.L.).

The systematic errors in P_2 given by uncertainties in detector acceptance, background levels, and the uncertainty in the $\rho\pi/f_2\pi$ branching ratio are estimated to contribute 4% each, for a total of 7%.

	I	II	III
Background [%]	0^*	23±4	23^*
P_2 [%]	–	77±12	74±13
$2^-(0)$ [%]	100^*	0^*	12±11
$P_{\gamma\gamma}$ [keV]	0.43±0.02	0.38±0.03	0.39±0.02
C.L. [%]	1.7×10^{-6}	57	61

Table 4: Parameters of fits to $\cos\theta$ distributions of π^0 and $\pi^\pm$. (*) parameter fixed in the fit.

3.3 Resonance parameters

The $m(\pi^+\pi^-\pi^0)$ mass spectrum in the region 1.0-2.1 GeV with $|\sum \vec{p}_T|^2 < 0.0015$ GeV^2 is fitted by minimizing a χ^2 function with expected value in bin i of :

$$E_i = \Gamma^{a_2}_{\gamma\gamma} \cdot M_i^{a_2} + BW_i + P_b \mathcal{B}_i^m. \tag{12}$$

The a_2 contribution, represented by $M_i^{a_2}$, is given by the Monte Carlo, assuming the PDG average values of the mass and width [9], and helicity 2 fraction $P_2 = 0.92$, as determined in Section 3.2 above. The a_2 contribution is scaled by the factor $\Gamma^{a_2}_{\gamma\gamma}$, which is a free parameter in the fit. The high-mass exclusive signal is described by the Breit-Wigner function:

$$BW = P_{BW} \cdot \frac{\Gamma_{tot}}{(m^2 - W^2_{\gamma\gamma})^2 + m^2\Gamma^2_{tot}}, \tag{13}$$

with fit parameters P_{BW}, Γ_{tot} and m. The inclusive background $\mathcal{B}_i^m$ is estimated from the fits to the $|\sum \vec{p}_T|^2$ distributions shown in Fig. 5. The shape is parameterized by a third order polynomial with the normalization P_b left free in the fit. The result of the fit is shown in Fig. 9, with $\chi^2 = 57$ for 42 D.F. (C.L.=6.1%).

The radiative widths for a_2 and the events in the high-mass region described by Eq. 13 are obtained from the fitted parameters $\Gamma^{a2}_{\gamma\gamma}$ and P_{BW}. The fitted widths are $\Gamma_{\gamma\gamma} = 0.98 \pm 0.05$ for the a_2 and $\Gamma_{\gamma\gamma} BR(\pi^+\pi^-\pi^0) = 0.29 \pm 0.04$ for the high-mass region assuming a single resonance. For the a_2, the radiative width is consistent with that obtained from the angular distribution (Section 3.2). The systematic errors in the radiative widths are due to uncertainties in acceptance, background, and branching ratios. For the a_2 these contributions are 3%, 4% and 7%, respectively; while for the high-mass region they are 4% for acceptance and 4% for background. These values are summarized in Table 5.

The fitted resonance parameters are corrected for the shift caused by the mass-dependent width and the calibration estimated by the Monte Carlo simulations. For the high-mass region the corrected mass is $m = 1752 \pm 21 \pm 4$ MeV. We also made a separate Breit-Wigner fit for the mass and width of the a_2. The mass is found to be $1323 \pm 4 \pm 3$ MeV. The mass resolution of the detector increases the Γ values obtained in the Breit-Wigner fits. This effect is calculated using Monte Carlo. The corrected widths are $\Gamma = 105 \pm 10 \pm 11$ MeV and $\Gamma = 150 \pm 110 \pm 34$ MeV for the a_2 and at 1750 MeV, respectively.

	$a_2(1320)$	high-mass region
$\Gamma_{\gamma\gamma}$ [keV]	$0.98 \pm 0.05 \pm 0.09$	–
$\Gamma_{\gamma\gamma} BR(\rho\pi + f_2\pi)$ [keV]	–	$0.29 \pm 0.04 \pm 0.02$
m [MeV]	$1323 \pm 4 \pm 3$	$1752 \pm 21 \pm 4$
Γ [MeV]	$105 \pm 10 \pm 11$	$150 \pm 110 \pm 34$

Table 5: The resonance parameters and the corresponding statistical and systematic errors.

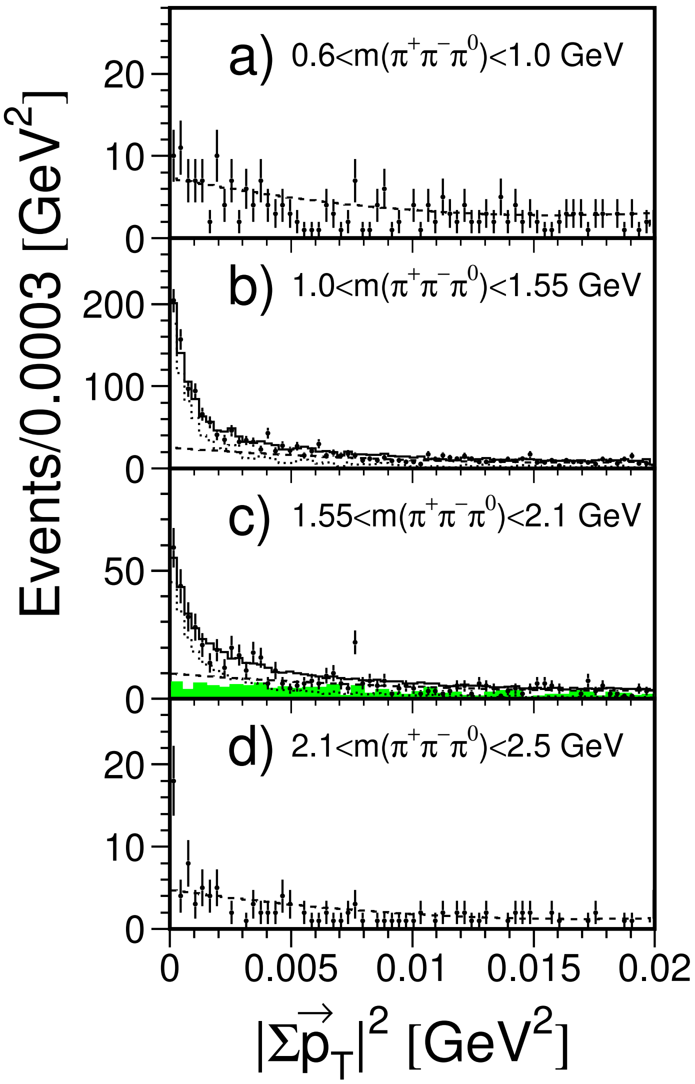

Figure 5: The $|\sum \vec{p}_T|^2$ distributions for $\pi^+\pi^-\pi^0$ events (points with statistical error) in different intervals of invariant mass. The $|\sum \vec{p}_T|^2$ distributions are fitted to background of second order polynomial (dashed line) and Monte Carlo predictions (dotted line) in b) and c) for exclusive resonance formation. The shaded histogram in c) is the distribution for a $\pi^+\pi^-\pi^0(\pi^0)$ phase space Monte Carlo sample normalized to the polynomial background estimate.

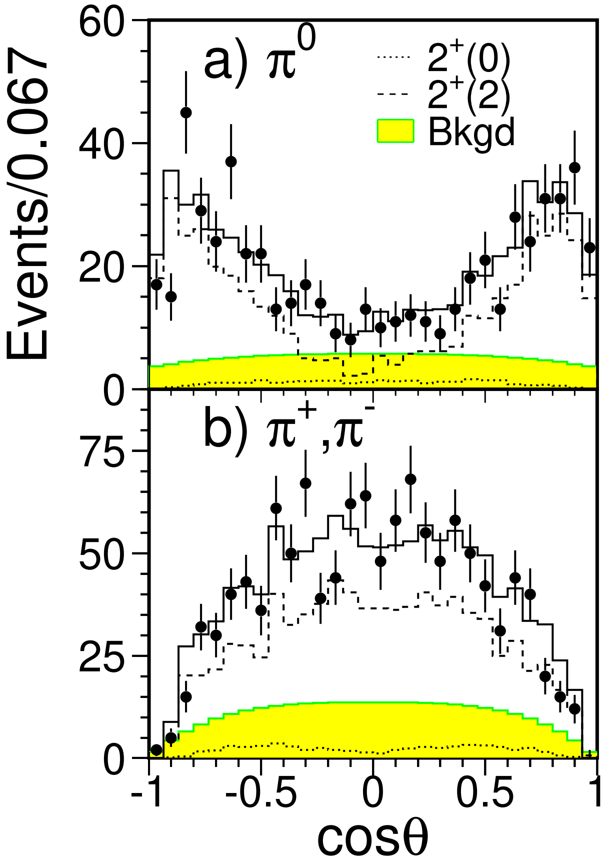

Figure 6: $\cos\theta$ distributions of a) π^0 and b) $\pi^\pm$ (two entries per event) for a_2 (points with statistical error) which are compared to the results of the fit (solid line). The dotted and dashed lines indicate the contributions for the two helicity states and the shaded area represents the background.

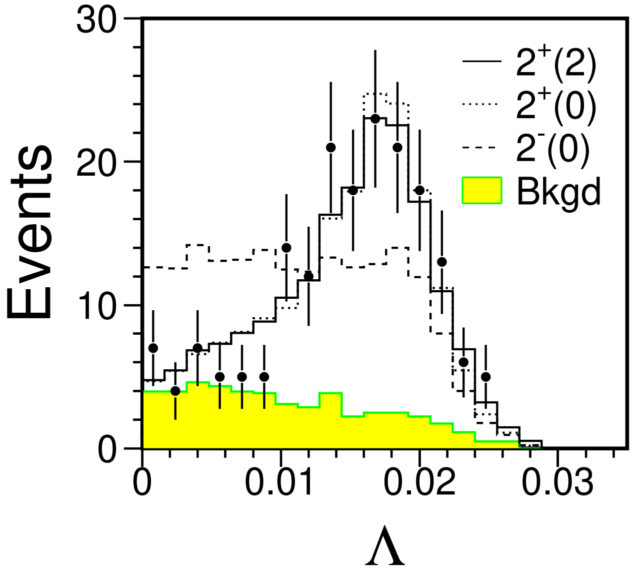

Figure 7: Λ distribution of data (points with statistical error) and Monte Carlo of $\mathrm{J^P}(\lambda) = 2^+(0)$ (dotted), $2^+(2)$ (solid), and $2^-(0)$ (dashed), respectively. A 25% inclusive background (shaded) is included using a phase space $\pi^+\pi^-\pi^0(\pi^0)$ distribution.

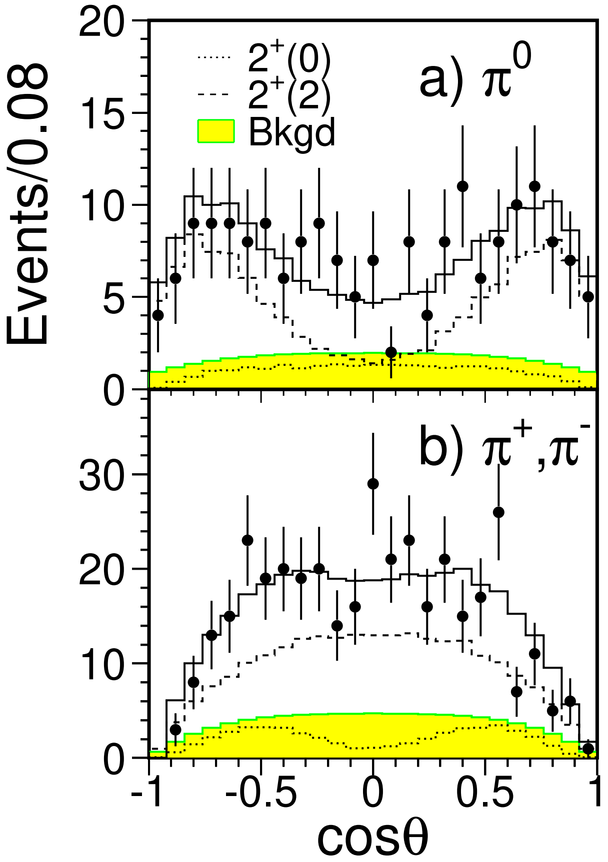

Figure 8: $\cos\theta$ distributions of a) π^0 and b) $\pi^\pm$ (two entries per event) for the *high-mass* selection (points with statistical error) which are compared to the results of the fit (solid line, column II of Table 4).

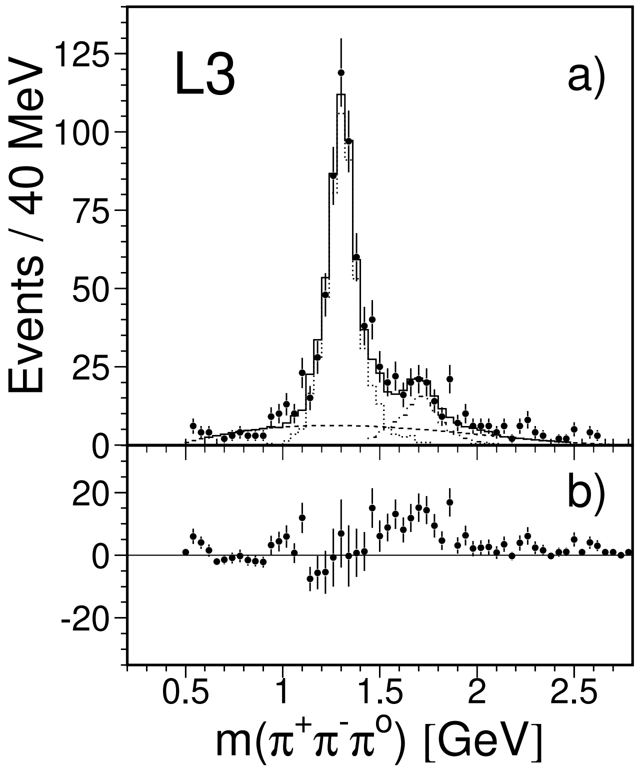

Figure 9: a) $\pi^+\pi^-\pi^0$ invariant mass spectrum; the solid line is the fit to the Monte Carlo sample for the a_2 (dotted line), a Breit-Wigner distribution in the high-mass region (dotted-dashed line) and a background parameterized by a third order polynomial (dashed line). b) the distribution with a_2 and background subtracted.

4 The $K_s^0 K_s^0$ final state

The reaction $e^+e^- \to e^+e^-\gamma^*\gamma^* \to e^+e^- K_s^0 K_s^0$ is studied using the full luminosity collected at center-of-mass energies around 91 GeV [19,20]. Only the $K_s^0 \to \pi^+\pi^-$ decay mode is considered. In order to study $\gamma\gamma \to K_s^0 K_s^0 \to \pi^+\pi^-\pi^+\pi^-$, we require:

- The total energy seen in the calorimeters must be smaller than 30 GeV to exclude annihilation events.
- There must be exactly four good charged tracks in the tracking chamber with a net charge of zero. A good track requires more than 20 hits out of a maximum of 62.
- Exclusive events are selected by requiring $|\vec{p}_T(\pi^+\pi^-\pi^+\pi^-)|^2 < 0.1$ GeV^2.
- Events with photons are rejected. A photon is defined as a shower in the electromagnetic calorimeter with an energy larger than 100 MeV. The signal must be present in more than two crystals, in order to reduce the noise contribution. The ratio between the energies deposited in the hadronic and electromagnetic calorimeters must be less than 0.2. There must be no charged track in a cone of 200 mrad around the photon direction.

The K_s^0's are identified by requiring a secondary vertex [21] distinct from the primary interaction point with a distance larger than 3 mm. The angle between the flight direction of each K_s^0 candidate and the total transverse momentum vector of the two outgoing tracks must be smaller than 0.3 rad.

Fig. 10 shows the $\pi^+\pi^-$ mass distribution with a 3 mm vertex cut for the K_s^0. Fitting this distribution, we find a mass resolution of $\sigma = 9.6 \pm 0.8$ MeV, consistent with the Monte Carlo simulation.

Fig. 11(a) shows m($\pi^+\pi^-$) at one secondary vertex versus m($\pi^+\pi^-$) at the other secondary vertex: a clear clustering is found corresponding to exclusive $K_s^0 K_s^0$ production over a little non-K_s^0 background. This background is found negligible by Monte Carlo and K_s^0 sideband studies. The masses of the two K_s^0 candidates must be within ± 25 MeV of the K_s^0 mass.

The $K_s^0 K_s^0$ mass spectrum (fig. 11(b)) shows clear evidence for the formation of the $f_2'(1525)$ tensor meson. The f_2-a_2 destructive interference around 1300 MeV is observed, according to theoretical predictions [22]. An enhancement is observed around 1750 MeV. Its statistical significance is 3 standard deviations. According to recent theoretical predictions [23], it is probably due to the formation of a radially excited state of the $f_2'(1525)$ tensor meson.

A maximum likelihood fit using two Gaussians and a flat background is then performed on the $K_s^0 K_s^0$ mass spectrum. The masses and widths of the Gaussians are left free in the fit. The fit is shown in fig. 11(b) and the results are summarized in Table 6.

	First peak $f_2'(1525)$	Second peak
Mass (MeV)	1515 ± 10	1760 ± 14
Width (MeV)	112 ± 19	119 ± 26

Table 6: Results from the maximum likelihood fit of the $K_s^0 K_s^0$ invariant mass spectrum.

For the $f_2'(1525)$ the detection and trigger efficiencies are evaluated by Monte Carlo simulation. All the events are passed through the full detector simulation program and are reconstructed following the same procedure used for the data. Although the detector acceptance is rather high (15% for helicity zero and 30% for helicity two), the trigger efficiency (83%), the data selection (72%) and the analysis cuts ($\sim$ 30%) give a total efficiency of 1.9% for helicity zero and 4.1% for helicity two. We measure $\Gamma_{\gamma\gamma}(f_2')BR(f_2' \to K\bar{K})$=0.093± 0.018± 0.022 keV under the hypothesis of a pure helicity-2 and $\Gamma_{\gamma\gamma}(f_2')BR(f_2' \to K\bar{K})$=0.198± 0.040± 0.050 keV for a pure helicity-0 state. The study of the angular distribution in the two-photon centre-of-mass system favors helicity-2 formation over helicity-0, according to theoretical predictions [24].

From the measurement of the radiative width of the $f_2'(1525)$, it is possible to determine the mixing angle θ between the singlet and the octet members of the tensor meson nonet using the relation

$$\frac{\Gamma_{\gamma\gamma}(f_2')}{\Gamma_{\gamma\gamma}(f_2)} = \frac{m^3_{f_2'}}{m^3_{f_2}} \cdot \frac{(\cos\theta - 2\sqrt{2}\sin\theta)^2}{(\sin\theta + 2\sqrt{2}\cos\theta)^2}. \tag{14}$$

Using the result of the present analysis and the PDG values for $BR(f_2' \to K\bar{K}) = (71.2^{+2.0}_{-2.5})\%$ and $\Gamma_{\gamma\gamma}(f_2) = (2.4 \pm 0.3)$ keV, a value of

$$\theta = (29.4^{+1.4}_{-1.6})^\circ$$

is obtained. The result indicates a deviation from ideal mixing ($\theta = 35.3^\circ$) and is in agreement with the value of $\theta = (28 \pm 3)^\circ$ found from the Gell-Mann$-$Okubo mass formula. Our result is also in agreement with the value of $\theta = (28 \pm 2)^\circ$ found in an analysis of the tensor nonet [25].

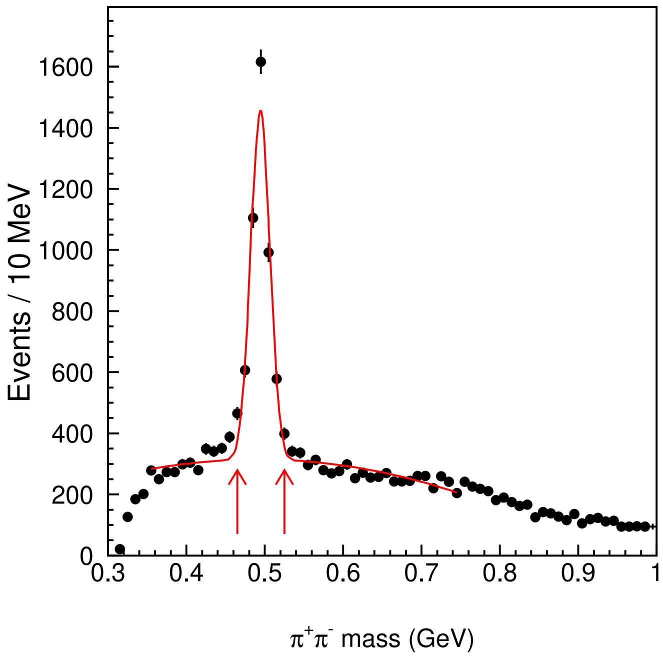

Figure 10: The $\pi^+\pi^-$ mass spectrum for reconstructed secondary vertices which are more than 3 mm from the interaction point. The curve is the result of a fit using a third-order polynomial for the background and a Gaussian for the peak. The arrows indicate the signal region.

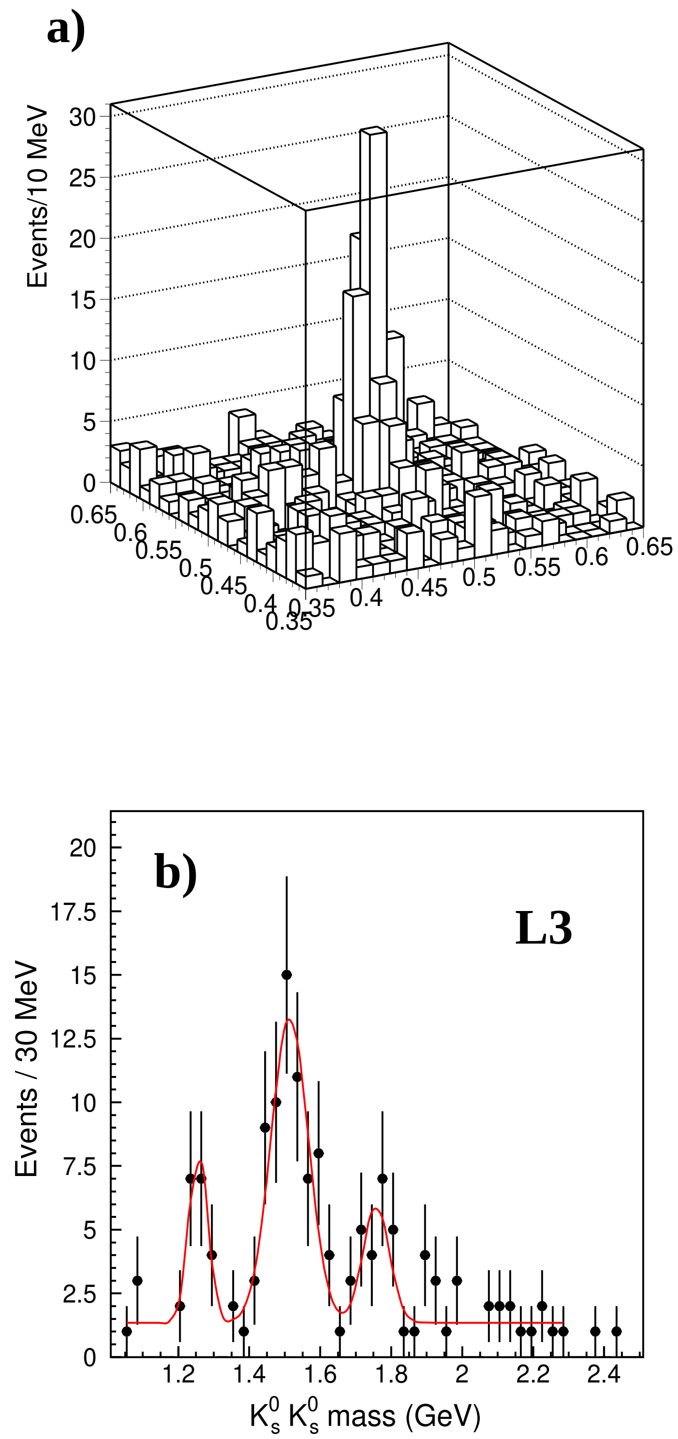

Figure 11: a) m($\pi^+\pi^-$) at one secondary vertex versus m($\pi^+\pi^-$) at the other secondary vertex. b) The $K_s^0 K_s^0$ mass spectrum.

5 The $\pi^+\pi^-$ and the K^+K^- Final States

In order to select exclusive two charged track events, we require two good tracks of opposite charge with a total transverse momentum squared smaller than 0.06 GeV^2. These events are dominated by $\gamma^*\gamma^* \to e^+e^-$ and $\gamma\gamma \to \mu^+\mu^-$. In order to identify different charged particles an artificial neural network technique has been developed using track momentum, ionization loss (dE/dx), electromagnetic and hadron calorimeter information. In fig. 12 mass spectra are shown for identified $\pi^+\pi^-$ and K^+K^- pairs. The $\pi^+\pi^-$ spectrum is dominated by the formation of the $f_2(1270)$ tensor meson. The K^+K^- spectrum shows f_2-a_2 constructive interference [22] around 1300 MeV and the formation of the $f_2'(1525)$ tensor meson.

6 Discussion and conclusions

A high statistics sample of $e^+e^- \to e^+e^-\eta'$, $\eta' \to \pi^+\pi^-\gamma$ events has been collected with the L3 detector at LEP energies around 91 GeV. The channel is dominated by $\eta' \to \rho\gamma$. We find no positive evidence for a box anomaly contribution. From the quasi-real two-photon interaction the η' radiative width $\Gamma_{\gamma\gamma}(\eta') = 4.17 \pm 0.10$ (stat.) $\pm$ 0.27 (sys.) keV is obtained. This value is the most precise obtained in a single experiment. It is consistent with the world average. The η' transition form factor has been measured in the interval $0.01 \leq Q^2 \leq 10.0$ GeV^2. A fit to the data with a pole parameterization gives a value $\Lambda = 0.900 \pm 0.046$ (stat.) $\pm$ 0.022 (sys.) GeV, which corresponds to the interaction size $\langle r^2 \rangle = 0.286 \pm 0.016$ fm^2. The pole form is a good representation of the data. The Vector Dominance Model and recent non-perturbative QCD calculations are consistent with these data.

The $\pi^+\pi^-\pi^0$ final state in two-photon collisions is found to be dominated by formation of the a_2 meson. The λ=2 helicity state is dominant. The $\pi^+\pi^-\pi^0$ events in the mass region 1.55-2.1 GeV have been analyzed for spin-parity and resonance parameters for spin up to J=2 and in intermediate states $\rho\pi$ and $f_2\pi$, the spin-parity are found to be dominated by J$^{\rm P}(\lambda)$ =2$^+$(2). Equal branching ratios for decays into the $f_2\pi$ and $\rho\pi$ final states are observed and the phase angle ϕ between the $\rho\pi$ and $f_2\pi$ amplitudes is consistent with 180°. The results may be compared with theoretical predictions, in particular the calculations of the relativistic quark model of Ref. [23]. If these events are identified with the first radial excitation of the a_2, the fitted mass $m = 1752 \pm 21 \pm 4$ MeV is consistent only with the One Gluon Exchange Semi-Relativistic Quark Mass (OGE-SRM) model which predicts a mass of 1740 MeV. The formation of a J$^{\rm P}$ = 2$^-$ state, π_2, claimed by previous collaborations [26, 27] was based solely on the 3π mass distribution and observation of $f_2\pi$ decay mode. No evidence is seen for this state. The upper limit $\Gamma_{\gamma\gamma}(\pi_2)BR(\pi^+\pi^-\pi^0) < 0.072$ keV (90% C.L.) is found. This result is in agreement with the ARGUS observation [28].

The radiative width measured for f_2' in $K^0_sK^0_s$ final state of helicity two is consistent with previous measurements [19]. In the $f_2(1270) - a_2(1320)$ mass region, the few amount of events observed is consistent with the theoretical prediction of destructive f_2-a_2 interference [22]. The $K^0_sK^0_s$ mass spectrum shows an enchancement near 1800 MeV. The mixing angle between the siglet and octet members fo the SU(3) tensor meson nonet is evaluated to be $\theta = 29.4^{+1.4}_{-1.6}$ degree.

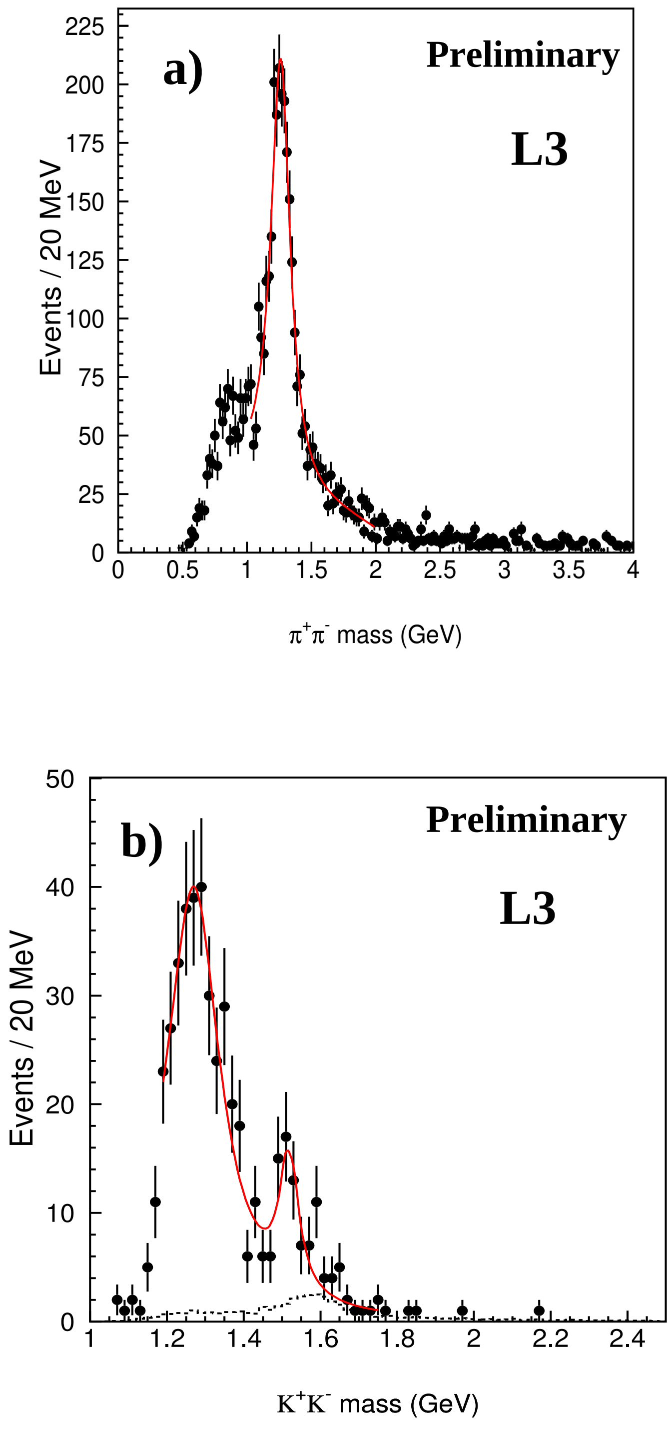

Figure 12: a) The $\pi^+\pi^-$ mass spectrum. b) The K^+K^- mass spectrum.

References

[1] L3 Collab., B. Adeva et al., Nucl. Inst. Meth. A 289 (1990) 35.

[2] V.M. Budnev et al., Phys. Rep. 15 (1975) 181.

[3] " Measurement of the $\eta'(958)$ formation in Two-Photon Collisions at LEP " L3 Collab., M. Acciarri et al., To be submitted to Phys. Lett. B.

[4] Ll. Ametler, J. Bijnens, A. Bramon, F. Cornet, Phys. Rev. D 45 (1992) 986 and references therein.

[5] S.I. Bityukov et al., Z. Phys. C 50 (1991) 451.

[6] M. Benayoun et al., Z. Phys. C 58 (1993) 31.

[7] Crystal Barrel Coll., A. Abele et al., Phys. Lett. B 402 (1997) 195.

[8] J.D. Jackson, Nuovo Cimento 34 (1964) 1644.

[9] Review of Particle Physics, Phys. Rev. D 54 (1996) 1.

[10] F.L. Linde, Ph.D. thesis (Rijksuniversiteit Leiden, 1988).

[11] S.J. Brodsky and G. P. Lepage, Phys. Rev. D 24 (1981) 1808.

[12] R. Jacob, P. Kroll and M. Raulfs, J. Phys. G 22 (1996) 45.

[13] V.V. Anisovich, D.I. Melikhov and V.A. Nikonov, Phys. Rev. D 55 (1997) 2918.

[14] V.V. Anisovich, D.V. Bugg, D.I. Melikhov and V.A. Nikonov, hep-ph/9702383, to be published in Phys. Lett. B.

[15] L3 Collab., M. Acciarri et al., CERN-PPE/97-68 (submitted to Phys. Lett. B), and references therein.

[16] W.R.Frazer et al., Phys. Rev. 136 (1964) B1207.

[17] A. Buijs et al., Comp. Phys. Comm. 79 (1994) 523.

[18] G. Goldhaber et al., Phys. Rev. Lett. 15 (1965) 118.

[19] L3 Collab., M. Acciarri et al., Phys. Lett. B 363 (1995) 118.

[20] S. Braccini, *"Studio delle interazioni fotone-fotone con il rivelatore L3 al LEP"*, Tesi di Laurea, University of Florence, Italy (1995).

[21] F. Becattini, Ph. D. Thesis, University of Florence, Italy (1996).

[22] H.J. Lipkin, Nucl. Phys. B 7 (1968) 321; Proc.s. EPS Int. Conf. Palermo 1975, p. 609; D. Faiman et al., Phys. Lett. B. 59 (1975) 269.

[23] E. Klempt, B.C. Metsch, C.R. Münz, H.R. Petry, Phys. Lett. B 361 (1995) 160; C.R. Münz, Nucl. Phys. A 609 (1996) 364.

[24] B. Schrempp-Otto et al., Phys. Lett. B 36 (1971) 463;
G. Köpp et al., Nucl. Phys. B 70 (1974) 461;
P. Grassberger and R. Kögerler, Nucl. Phys. B 106 (1976) 451.

[25] K. Peters and E. Klempt, Phys. Lett. B 352 (1995) 467.

[26] Crystal Ball Collab., D. Antreasyan et al., Z. Phys. C 48 (1990) 561.

[27] CELLO Collab., H.J. Behrend et al., Z. Phys. C 46 (1990) 583.

[28] ARGUS Collab., H. Albrecht et al., DESY 96-015 Jan. 1996; DESY 96-112 Jun. 1996.